Acta Crystallographica Section D
Biological Crystallography
ISSN 1399-0047

The structure of the proteinaceous inhibitor PliI from *Aeromonas hydrophila* in complex with its target lysozyme

Seppe Leysen,[a]‡ Joris M. Van Herreweghe,[b] Kazunari Yoneda,[c] Makoto Ogata,[d] Taichi Usui,[e] Tomohiro Araki,[c] Christiaan W. Michiels[b] and Sergei V. Strelkov[a]*

[a]Laboratory for Biocrystallography, Department of Pharmaceutical and Pharmacological Sciences, KU Leuven, 3000 Leuven, Belgium, [b]Laboratory of Food Microbiology, Leuven Food Science and Nutrition Research Centre, KU Leuven, 3000 Leuven, Belgium, [c]Department of Bioscience, School of Agriculture, Tokai University, Kawayo, Minamiaso, Kumamoto 869-1404, Japan, [d]Department of Chemistry and Biochemistry, Fukushima National College of Technology, 30 Nagao, Kamiarakawa, Taira, Iwaki, Fukushima 970-8034, Japan, and [e]Department of Bioscience, Graduate School of Science and Technology, Shizuoka University, 836 Ohya, Suruga, Shizuoka 422-8529, Japan

‡ Current address: Technische Universiteit Eindhoven, The Netherlands.

Correspondence e-mail: sergei.strelkov@pharm.kuleuven.be

Received 2 July 2014
Accepted 26 November 2014

PDB reference: PliI–lysozyme complex, 4pj2

Recent microbiological data have revealed that Gram-negative bacteria are able to protect themselves against the lytic action of host lysozymes by secreting proteinaceous inhibitors. Four distinct classes of such inhibitors have been discovered that specifically act against c-type, g-type and i-type lysozymes. Here, the 1.24 Å resolution crystal structure of the periplasmic i-type lysozyme inhibitor from *Aeromonas hydrophila* (PliI-Ah) in complex with the i-type lysozyme from *Meretrix lusoria* is reported. The structure is the first to explain the inhibitory mechanism of the PliI family at the atomic level. A distinct 'ridge' formed by three exposed PliI loops inserts into the substrate-binding groove of the lysozyme, resulting in a complementary 'key–lock' interface. The interface is principally stabilized by the interactions made by the PliI-Ah residues Ser104 and Tyr107 belonging to the conserved SG*x*Y motif, as well as by the other conserved residues Ser46 and Asp76. The functional importance of these residues is confirmed by inhibition assays with the corresponding point mutants of PliI-Ah. The accumulated structural data on lysozyme–inhibitor complexes from several classes indicate that in all cases an extensive interface of either a single or a double 'key–lock' type is formed, resulting in highly efficient inhibition. These data provide a basis for the rational development of a new class of antibacterial drugs.

1. Introduction

In the animal kingdom, lysozymes are important enzymes of the innate immune system. Three major types of animal lysozymes can be discriminated based on their primary sequences. They are designated as c-type (chicken or common type), g-type (goose type) and i-type (invertebrate type). The lysozymes exert a strong antibacterial activity by undermining the structural integrity of the bacterial cell wall, ultimately leading to osmotic lysis. In particular, they catalyse hydrolysis of the β(1–4) glycosidic bond between *N*-acetylmuramic acid (NAM) and *N*-acetylglucosamine (NAG), which are the disaccharide building blocks of the peptidoglycan layer of the cell wall. In their substrate-binding cleft, lysozymes have six subsites for binding NAG and/or NAM molecules. These subsites are labelled A–F for c-type and i-type lysozymes and B–G for g-type lysozymes. Peptidoglycan cleavage ultimately occurs between the NAM and NAG molecules occupying subsites D and E (see, for example, Callewaert & Michiels, 2010; Van Herreweghe & Michiels, 2012).

From their side, bacteria have developed strategies to protect their peptidoglycan layer against the lytic action of their host's lysozymes. A well known strategy is the introduction of chemical modifications into the peptidoglycan

backbone (reviewed in Davis & Weiser, 2011), while a more recently discovered strategy is the production of proteinaceous lysozyme inhibitors. To date, four distinct lysozyme inhibitor families have been described (reviewed in Callewaert *et al.*, 2012). Initially the Ivy (inhibitor of vertebrate lysozyme) family was identified (Monchois *et al.*, 2001), and was soon followed by three other lysozyme inhibitor families designated MliC/PliC (membrane-associated/periplasmic lysozyme inhibitor of c-type lysozyme), PliG (periplasmic lysozyme inhibitor of g-type lysozyme) and PliI (periplasmic lysozyme inhibitor of i-type lysozyme) (Callewaert *et al.*, 2008; Van Herreweghe *et al.*, 2010; Vanderkelen *et al.*, 2011).

In the past, X-ray structure determination of the complexes formed by Ivy, MliC/PliC and PliG with their respective lysozymes has helped to explain their inhibitory mechanisms (Leysen *et al.*, 2013; Yum *et al.*, 2009; Abergel *et al.*, 2007; Um *et al.*, 2013). Recently, we have also determined the crystal structure of PliI from *Aeromonas hydrophila* (PliI-Ah) and explored its inhibitory action on the i-type lysozyme from the clam *Venerupis philippinarum* (formerly known as *Tapes japonica*; Vp-iLys; Leysen *et al.*, 2011). Here, we describe the crystallographic complex of PliI-Ah with the i-type lysozyme from the closely related clam *Meretrix lusoria* (Ml-iLys). This structure is the first to explain the inhibitory mechanism of the PliI family at the atomic level.

2. Materials and methods

2.1. Protein purification

A pET-26b(+)-based construct expressing the PliI-Ah gene (Van Herreweghe *et al.*, 2010) was introduced into *Escherichia coli* BL21(DE3) cells by heat-shock transformation. A single colony was used to inoculate 1 ml LB containing 100 µg ml^{-1} ampicillin. After 8 h incubation at 37°C, 500 µl of this preculture was used to inoculate 1 l ZYP-5052 auto-induction medium (Studier, 2005) containing 100 µg ml^{-1} ampicillin and 0.1%(*v*/*v*) antifoam SE-15 (Sigma–Aldrich). The culture was grown at 24°C until it reached an $OD_{600\ nm}$ of 4.0. At this point, the temperature was decreased to 18°C and the culture was allowed to grow for an additional 24 h. The cells were pelleted by centrifugation, resuspended in 50 m*M* sodium phosphate, 250 m*M* NaCl, 12.5 m*M* imidazole pH 7.5 (IMAC12.5 buffer) and lysed using an EmulsiFlex-C5 homogenizer (Avestin) followed by sonication for 4 min with 60% amplitude and 1 s on/off pulses. The lysate was clarified by centrifugation. The supernatant containing PliI-Ah with a vector-encoded C-terminal Leu-Glu-$(His)_6$ tag was loaded onto a 3 ml nickel-chelating column (His60 Ni Superflow resin, Clontech) equilibrated with IMAC12.5 buffer. The column was washed with three column volumes of this buffer containing 0.1%(*v*/*v*) Triton X-100 followed by a further three column volumes of the buffer without detergent. PliI-Ah was eluted from the column with ten column volumes of 50 m*M* sodium phosphate, 250 m*M* NaCl, 250 m*M* imidazole pH 7.5 while collecting 1 ml fractions. The fractions containing PliI-Ah were combined and dialysed overnight at 4°C against 20 m*M* bis-tris pH 7.0, 10%(*w*/*v*) glycerol. Next, PliI-Ah was loaded onto a HiTrap Q HP column (GE Healthcare) equilibrated with 20 m*M* bis-tris pH 7.0 and a linear gradient of 0–400 m*M* NaCl (0–40% of a buffer consisting of 20 m*M* bis-tris pH 7.0, 1 *M* NaCl) was applied over 20 column volumes. Fractions containing PliI-Ah were pooled and concentrated using an Amicon ultracentrifugation device with a 3 kDa cutoff (Millipore). Finally, PliI-Ah was further purified by size-exclusion chromatography on a Superdex 75 pg 16/60 column (GE Healthcare) equilibrated with 10 m*M* Tris–HCl, 0.5 m*M* EDTA, 250 m*M* KCl pH 7.5 (SEC buffer).

Ml-iLys (an isoform with a Thr residue at position 5) was purified from clams as described in Kuwano, Yoneda, Kawaguchi, Araki *et al.* (2013). The purification of Vp-iLys was performed as described in Van Herreweghe *et al.* (2010).

2.2. Crystallographic analysis

The PliI-Ah–Ml-iLys complex was formed by mixing the proteins in equimolar amounts in SEC buffer. The complex was concentrated to 9.5 mg ml^{-1} using an Amicon ultracentrifugation device with a 3 kDa cutoff (Millipore). The protein concentration was determined by measuring the absorbance at 280 nm. To screen for crystallization conditions, the commercially available Index (Hampton Research) and PACT (Qiagen) kits were used. Trials were set up using the sitting-drop technique in MRC-type 96-well crystallization plates (Molecular Dimensions). For each condition, 100 nl protein-complex solution was mixed with an equal amount of precipitant solution. The best crystals were obtained after 3 d at 20°C with 0.1 *M* DL-malic acid/MES/Tris base cocktail buffer (MMT buffer as described in the Qiagen protocol), 25%(*w*/*v*) PEG 1500. A crystal measuring roughly 60 × 70 × 30 µm was transferred to precipitant solution supplemented with 20% glycerol and flash-cooled in liquid nitrogen. Diffraction data were collected at 100 K on the PROXIMA1 beamline at the SOLEIL synchrotron, France. The data sets were indexed and integrated using *XDS* (Kabsch, 2010) and scaled using *SCALA* (Evans, 2006). The structure was phased by molecular replacement in *Phaser* (McCoy *et al.*, 2007) using the structures of Ml-iLys (PDB entry 3ab6; Kuwano, Yoneda, Kawaguchi & Araki, 2013) and PliI-Ah (PDB entry 3od9; Leysen *et al.*, 2011) as search models. Iterative rounds of manual building using *Coot* (Emsley & Cowtan, 2004) and refinement employing the *PHENIX* package (Adams *et al.*, 2010) were used to complete the atomic model. The final atomic coordinates and the experimental structure factors were deposited in the Protein Data Bank under accession code 4pj2. Analysis of the PliI-Ah–Ml-iLys complex interface was performed using the *PISA* web server (Krissinel & Henrick, 2007).

2.3. Assays with designed PliI-Ah mutants

Generation of the PliI-Ah S104A/Y107A double mutant has been described previously (Leysen *et al.*, 2011). Using the same procedure, alanine substitutions were introduced to create the mutants S46A, D76A, S46A/S104A/Y107A, D76A/S104A/Y107A and S46A/D76A/S104A/Y107A. The primer

Table 1
Crystallographic statistics.

Values in parentheses are for the highest resolution shell.

PDB code	4pj2
Data collection	
Wavelength (Å)	0.9791
Resolution range (Å)	66–1.24 (1.31–1.24)
Space group	$P2_1$
Unit-cell parameters (Å, °)	a = 132.2, b = 77.7, c = 42.9, β = 108.1
Solvent content (%)	49
$CC_{1/2}$†	0.999 (0.619)
R_{merge}‡	0.050 (0.839)
R_{meas}§	0.057 (0.958)
$\langle I/\sigma(I)\rangle$	10.8 (1.7)
Completeness (%)	95.7 (89.8)
No. of unique reflections	144072
Multiplicity	4.3 (4.2)
Wilson B factor (Å^2)	15.6
Refinement	
Resolution range used (Å)	47.8–1.24
Total No. of reflections used	144031
No. of reflections in the 'free' set	1457
No. of non-H protein solvent atoms	3874/560
R_{work}	0.148
R_{free}	0.168
CC_{work}¶	0.966
CC_{free}¶	0.966
R.m.s. deviations from ideal values††	
Bond lengths (Å)	0.008
Bond angles (°)	1.2
Average B factor (Å^2)	
Protein	20.8
Solvent	33.8
Ramachandran plot‡‡	
Favoured (%)	98.6
Outliers (%)	0
MolProbity score/percentile‡‡	1.35/88
Clashscore/percentile‡‡	3.74/91
Good rotamers‡‡ (%)	98.2

† $CC_{1/2}$ is Pearson's intra-data-set correlation coefficient as described in Karplus & Diederichs (2012). ‡ $R_{merge} = \sum_{hkl}\sum_i |I_i(hkl) - \langle I(hkl)\rangle| / \sum_{hkl}\sum_i I_i(hkl)$, where $I_i(hkl)$ is the intensity of the ith observation of reflection hkl and $\langle I(hkl)\rangle$ is the average intensity of reflection hkl. § $R_{meas} = \sum_{hkl}\{N(hkl)/[N(hkl)-1]\}^{1/2} \sum_i |I_i(hkl) - \langle I(hkl)\rangle| / \sum_{hkl}\sum_i I_i(hkl)$, where $N(hkl)$ is the number of observations of reflection hkl. ¶ Correlation of experimental intensities with intensities calculated from the refined model as described in Karplus & Diederichs (2012) †† As described in Engh & Huber (1991). ‡‡ As calculated using *MolProbity* (Chen *et al.*, 2010).

sequences were S46A-Fw (forward), GGCGAACCTGCC-**GCC**ACCGGCAGCTACG, S46A-Rv (reverse), GCGCCCT-CTGCTGACGGTCACTACCTGGCCTGAGG, D76A-Fw, GTGCTGCCGCGC**GCT**GGCAGCATCAAGG, and D76A-Rv, CTTGCCGTCGATGAACTGATCCAGCGGGAACTG-GGGGTT. Vp-iLys lytic activity and the inhibition of this activity by wild-type and mutant PliI-Ah were measured as described previously (Van Herreweghe *et al.*, 2010). Briefly, lyophilized *Micrococcus luteus* cells (Sigma–Aldrich) were resuspended at 0.8 mg ml^{-1} in 10 m*M* potassium phosphate buffer pH 7.0. Thereafter, the cell lysis induced by the addition of Vp-iLys alone or together with a PliI-Ah variant was monitored at 30°C using a Bioscreen C Microbiology Reader (Labsystems Oy, Helsinki, Finland). The efficiency of inhibition was calculated as $I = [(L_0 - L) - (R_0 - R)]/[(L_0 - L) - (B_0 - B)]$, where $L_0 - L$ is the decrease in the $OD_{600\,nm}$ reading over 2 h upon the addition of lysozyme alone, $R_0 - R$ is the equivalent decrease upon the addition of both lysozyme and the inhibitor and $B_0 - B$ is the decrease after the addition of buffer only. The amount of added lysozyme was 0.55 µg ml^{-1} such that the $OD_{600\,nm}$ decrease with lysozyme alone was ∼0.5 in 2 h. The amount of the inhibitor was adjusted such that the inhibition efficiency was ∼50%. The relative activity of each mutant was then calculated as the ratio of the concentration-normalized inhibition efficiencies of the mutant and wild-type PliI-Ah.

3. Results and discussion

3.1. Crystal structure determination of the PliI-Ah–MI-iLys complex

We have recently reported that PliI-Ah forms a very tight complex with an i-type lysozyme from *V. philippinarium* (Vp-iLys). Using surface plasmon resonance (SPR), this interaction was found to have a K_d of 47 p*M* (Leysen *et al.*, 2011). For these experiments, Vp-iLys was produced recombinantly in *Pichia pastoris*, but the small yields were insufficient for crystallographic studies. Here, we have used a closely related i-type lysozyme from another clam, *M. lusoria* (Ml-iLys), that can be readily purified directly from the animal tissue in milligram amounts (Kuwano, Yoneda, Kawaguchi, Araki *et al.*, 2013). Ml-iLys and Vp-iLys share 65% amino-acid identity (Kuwano, Yoneda, Kawaguchi, Araki *et al.*, 2013). In line with this, their atomic structures are readily superimposable, yielding a root-mean-square deviation (r.m.s.d.) of 0.59 Å over 122 C$^\alpha$ atom pairs (Kuwano, Yoneda, Kawaguchi & Araki, 2013).

The complex of recombinantly produced PliI-Ah and tissue-purified Ml-iLys could be readily formed upon mixing the proteins in equimolar amounts and successfully crystallized. The structure has been determined to 1.24 Å resolution (Table 1). This surpasses the diffraction quality of both PliI-Ah (Leysen *et al.*, 2011; PDB entry 3od9, resolution 1.41 Å) and Ml-iLys (Kuwano, Yoneda, Kawaguchi & Araki, 2013; PDB entry 3ab6, resolution 1.78 Å) alone. Moreover, such diffraction quality is outstanding for a protein–protein complex. An automated search of the PDB indicates that there are only 164 entries (0.17% of the PDB) resolved at 1.24 Å resolution or better and containing more than one distinct polypeptide chain in the asymmetric unit. Manual examination of these entries reveals that the majority of them are protein–peptide complexes, with only a few being true protein–protein complexes, including the complex of PliG-Ec with Atlantic salmon g-type lysozyme at 0.95 Å resolution (Leysen *et al.*, 2013; Yum *et al.*, 2009). The high quality of the Ml-iLys–PliI-Ah complex crystals may reflect the compact, highly ordered structure of either component as well as their tight interaction.

3.2. Molecular basis of the inhibition of MI-iLys by PliI-Ah

There is one PliI-Ah dimer binding two Ml-iLys molecules per asymmetric unit of the crystals, resulting in an arrangement with twofold noncrystallographic symmetry (Fig. 1*a*). Each MI-iLys molecule makes contacts with both chains of the

PliI-Ah dimer, but the contact with one of the chains is more extensive. The larger contact, referred to here as the 'primary interface', essentially includes PliI-Ah loops 2, 4 and 6. In addition, a smaller 'secondary interface' involves loop 3 of the

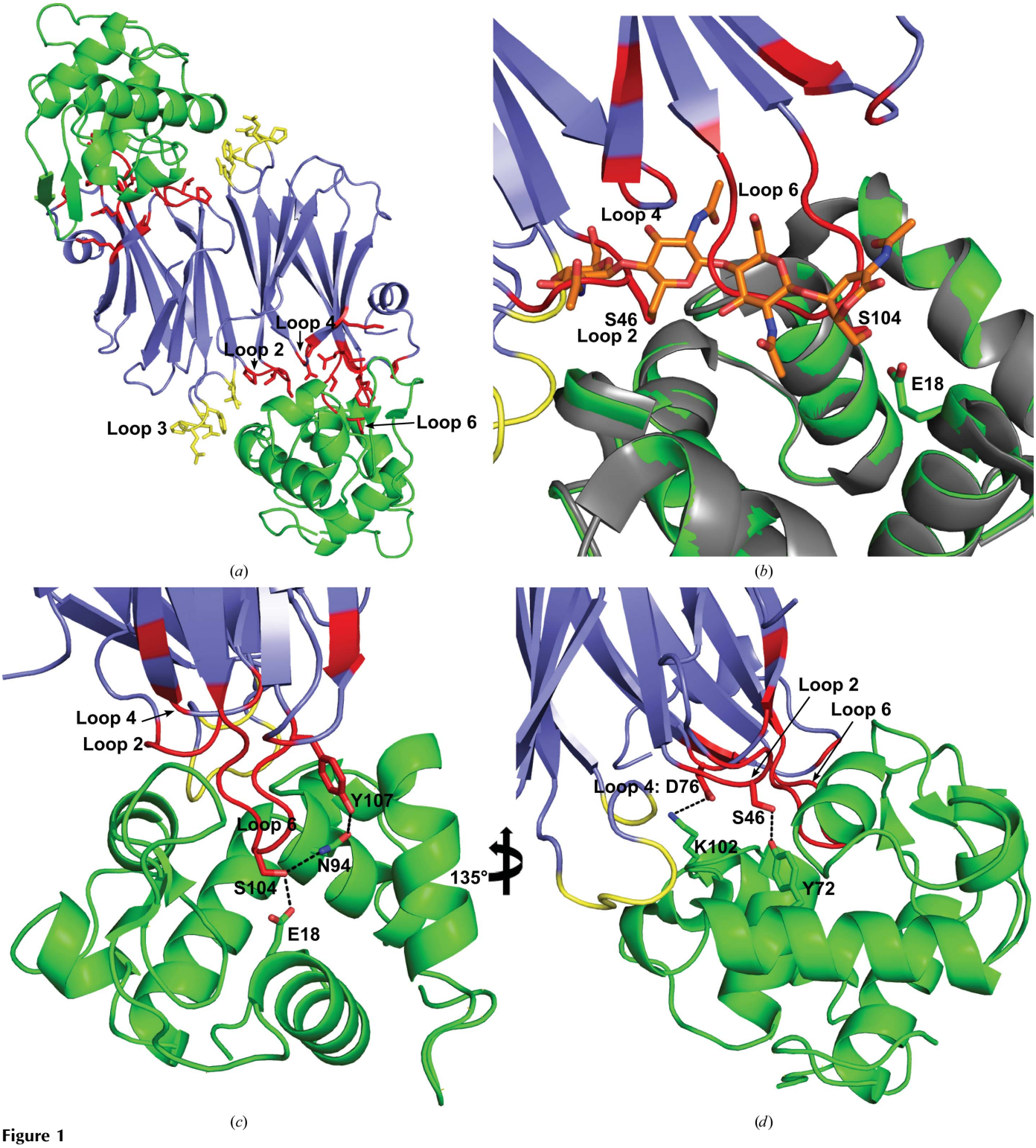

Figure 1
The PliI-Ah–Ml-iLys complex. (*a*) Asymmetric unit of the crystals containing the PliI-Ah dimer (blue) and two lysozyme molecules (green). The PliI-Ah residues involved in the primary interface (shown in red) are predominantly situated in loops 2, 4 and 6. The residues involved in the secondary interface (shown in yellow) are in loop 3. (*b*) A close-up of the active site of MI-iLys in two superimposed structures: in complex with PliI-Ah (lysozyme shown in green) and in complex with the substrate-like inhibitor 2,3-dideoxy-*N*,*N*′,*N*″,*N*‴-tetraacetylchitotetraose-1,5-lactone (PDB entry 3ayq; inhibitor in orange, lysozyme in grey). Loops 2, 4 and 6 occupy the substrate-binding groove, with the side chains of residues Ser46 and Ser104 matching the hydroxyl moieties of the substrate-like inhibitor. (*c*, *d*) Close-up view of the primary PliI-Ah–Ml-iLys interface shown in two different orientations. Key interactions are shown as dashed lines.

other PliI-Ah chain in the dimer (Fig. 1*a*). The primary and secondary interfaces measure about 730 and 240 Å^2, respectively. Here, the calculated values were rounded up to 10 Å^2 to reflect the practically achievable precision (Novotny *et al.*, 2007). The total interface area (970 Å^2) is comparable to that found in the lysozyme complexes of *E. coli* PliG (1200 Å^2), *Pseudomonas aeruginosa* MliC (960 Å^2) and *P. aeruginosa* Ivy (940 Å^2) (Abergel *et al.*, 2007; Leysen *et al.*, 2013; Yum *et al.*, 2009). It should also be noted that Ml-iLys–PliI-Ah complex formation buries substantial fractions (15 and 14%) of the solvent-accessible surfaces of the lysozyme and the inhibitor, respectively.

The main contribution to the primary interface is owing to PliI-Ah loop 6 (residues 101–107), which inserts into the active site of the lysozyme, in line with our earlier hypothesis (Leysen *et al.*, 2011). This loop contains the GSG*x*Y sequence that is highly conserved across PliI molecules from various bacterial species (Fig. 2). An SG*x*Y motif is also found in the PliG family members, whereas a closely related SG*xx*Y motif is present in the PliC/MliC family (Callewaert *et al.*, 2012). The detailed conformation of loop 6 together with the supporting electron density is given in Supplementary Fig. S1. The binding of loop 6 is responsible for 48% of the total area buried upon complex formation. In addition, loops 2 and 4 are also involved. Together, the three loops form a 'ridge' that inserts into the substrate-binding groove of the lysozyme (Fig. 1*d*). The specific interactions at the primary interface include 11 hydrogen bonds and a salt bridge (Table 2). Here, it is most illustrative to superimpose one Ml-iLys–PliI-Ah complex onto the recently determined structure of Ml-iLys in complex with the substrate analogue 2,3-dideoxy-*N*,*N*′,*N*″,*N*‴-tetraacetylchitotetraose-1,5-lactone (PDB entry 3ayq; K. Yoneda, Y. Kuwano, T. Usui, M. Ogata, A. Suzuki & T. Araki, unpublished work). The latter contains four consecutive glucose-based moieties that occupy substrate subsites A–D in the groove. Comparison of the structures readily reveals that PliI loops 2, 4 and 6 block these four subsites (Fig. 1*b*). Moreover, PliI-Ah residues Ser46 (loop 2) and Ser104 (loop 6) directly contribute to mimicking the substrate, as their hydroxyl side groups match the C_6-bound hydroxyls of sugar moieties in subsites B and D, respectively (Fig. 1*b*).

Atomic coordinate superpositions with the component structures reveal that Ml-iLys–PliI-Ah complex formation does not change the overall conformation of either protein (Supplementary Fig. S2). Indeed, a substrate-bound Ml-iLys structure (PDB entry 3ab6; Kuwano *et al.*, 2013) can be aligned with that in our complex with a C$^\alpha$ r.m.s.d. of ∼0.4 Å (0.46 and 0.29 Å for the two lysozyme copies in the complex, respectively) over 118 aligned residues (defined as residues deviating by less than 2 Å upon superposition as calculated with the *MatchMaker* tool in *Chimera*; Pettersen *et al.*, 2004). Unbound PliI-Ah (PDB entry 3od9;

Table 2
Hydrogen bonds (H) and salt bridges (SB) made by the PliI loops (primary interface).

PliI-Ah atom	Bond type	Ml-iLys atom
Loop 2		
Ala45 O	H	Asp47 O$^{\delta1}$
Ser46 O$^{\gamma}$	H	Asp47 O$^{\delta2}$
Ser46 O$^{\gamma}$	H	Tyr72 O$^{\eta}$
Loop 4		
Asp76 O$^{\delta2}$	SB	Lys102 N$^{\zeta}$
Loop 6		
Glu100 O$^{\varepsilon1}$	H	Ser32 O$^{\gamma}$
Ser101 O	H	Lys41 N$^{\zeta}$
Ser104 O$^{\gamma}$	H	Glu18 O$^{\varepsilon2}$
Ser104 O$^{\gamma}$	H	Asn94 N$^{\varepsilon2}$
Ser104 N	H	His93 O
Gly105 N	H	Asn94 O
Ser106 O$^{\gamma}$	H	Lys41 N$^{\zeta}$
Tyr107 O$^{\zeta}$	H	Asn94 O$^{\delta1}$

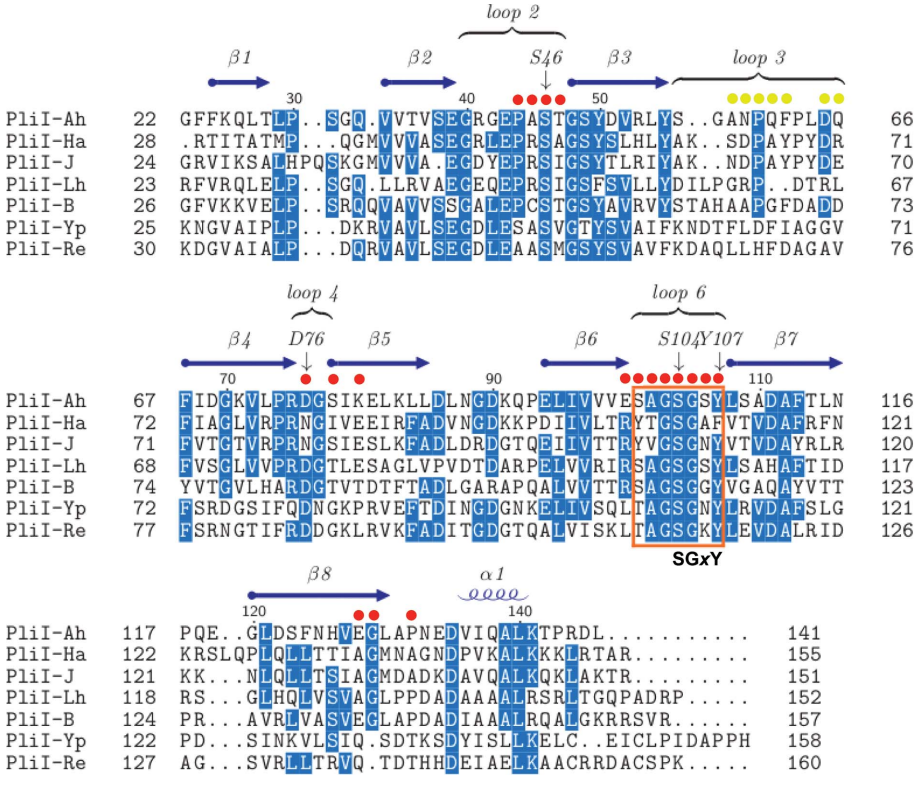

Figure 2
Multiple sequence alignment of the PliI family. The following species abbreviations are used: Ah, *A. hydrophila*; Ha, *Herminiimonas arsenicoxydans*; J, *Janthinobacterium* sp. Marseille; Lh, *Laribacter hongkongensis*; B, *Burkholderia* sp. 383; Yp, *Yersinia pestis*; Re, *Ralstonia eutropha*. Secondary-structure elements of PliI-Ah are indicated above the alignment. Loop 6 containing the conserved motif SG*x*Y is boxed. PliI-Ah amino acids which are part of the primary and secondary interface with Ml-iLys are marked with red and yellow dots, respectively. The alignment was created using *STRAP* (Gille & Frömmel, 2001).

Leysen *et al.*, 2011) can be aligned with the PliI-Ah molecules in the complex with a C^{α} r.m.s.d. of ∼0.6 Å over 118 residue pairs. At the same time, there is a pronounced local conformation change in the lysozyme near its active site caused by insertion of loop 6 of the inhibitor. The β-hairpin holding the catalytic residue Asp29 of the lysozyme is pushed outwards, resulting in a 4.5 Å movement of its C^{α} position compared with the substrate-bound state (Supplementary Fig. S2).

The secondary interface between the PliI-Ah dimer and each bound lysozyme molecule involves loop 3 of the inhibitor (Fig. 1*a* and Supplementary Fig. S3). Here, PliI-Ah residue Asp65 makes a salt bridge with Arg75 of the lysozyme, PliI-Ah residue Asn66 is hydrogen-bonded to the main-chain carboxyl of Ml-iLys Trp79, and PliI-Ah residue Ala68 packs against the aromatic group of the same residue. Comparison with other PliI species (Fig. 2) shows that the sequences of loop 2, loop 4 and especially loop 6 (all contributing to the primary interface) are quite conserved. In contrast, the sequence of loop 3 is not conserved. At the same time, the secondary interface still contributes about 25% of the total interface area and its role should be further investigated.

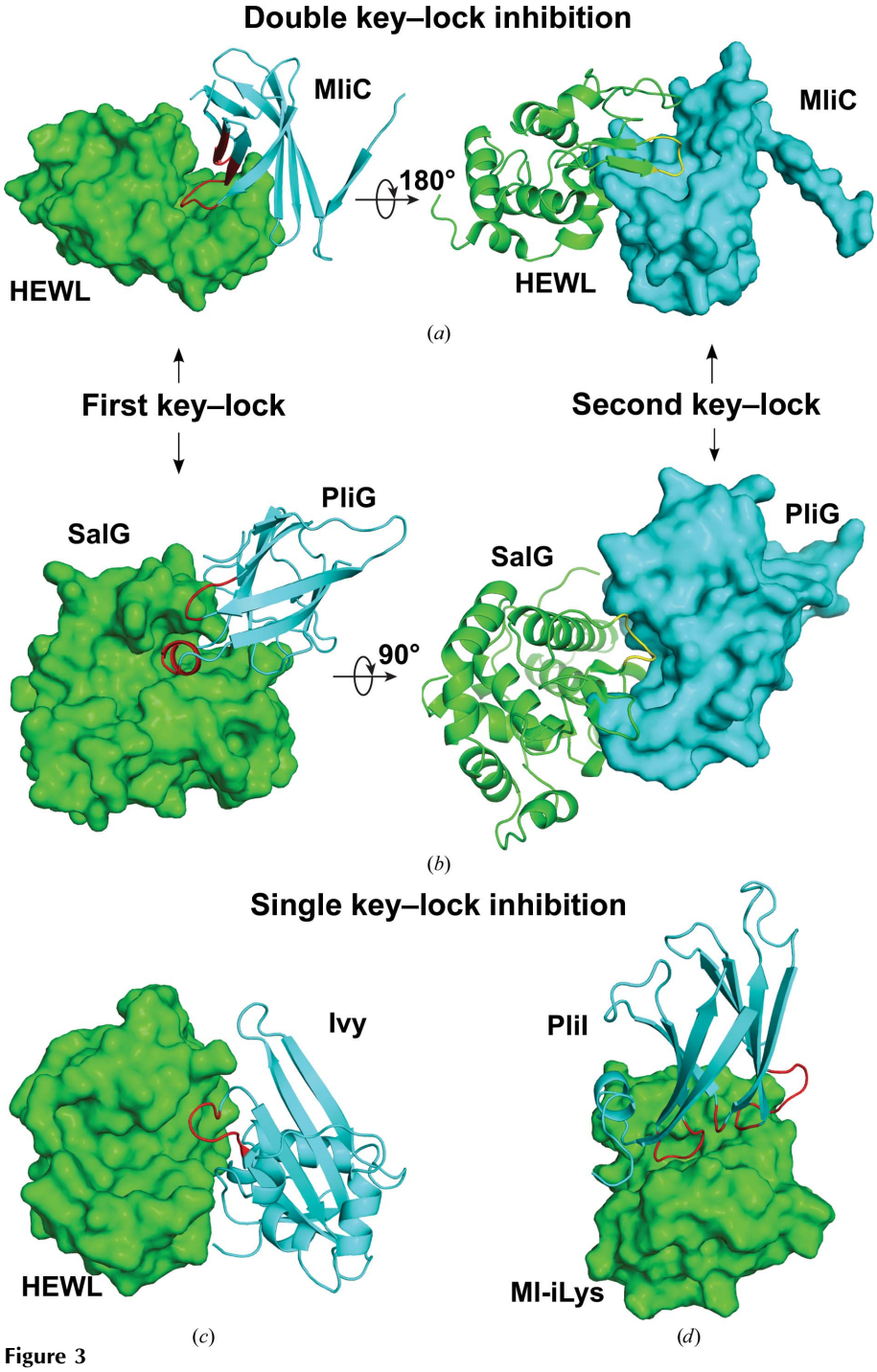

Figure 3
Comparison of the inhibitory complexes formed by the MliC/PliC, PliG, Ivy and PliI families. The inhibitors are shown in cyan as a cartoon with the inserting 'key' element in red or as a surface representation. Their target lysozymes are shown in green as surfaces or as cartoons with the inserting 'key' in yellow. (*a*) The crystal structure of *P. aeruginosa* MliC in complex with HEWL (PDB entry 3f6z; Yum *et al.*, 2009). For clarity, only one chain of the dimeric inhibitor, together with the bound lysozyme, is shown. The two 180° rotated views show the first and second key–lock interfaces. (*b*) The crystal structure of Ec-PliG in complex with salmon g-type lysozyme (PDB entry 4g9s; Leysen *et al.*, 2013). This inhibitor is monomeric. The two views show the first and second key–lock interfaces. (*c*) The crystal structure of the Ivy-Ec–HEWL complex (PDB entry 1gpq; Abergel *et al.*, 2007). Only one chain of the dimeric inhibitor, together with the bound lysozyme, is shown, revealing a single key–lock interface. (*d*) The single key–lock pair of the PliI-Ah–Ml-iLys complex.

3.3. Mutagenesis studies of the interaction interface

We have shown previously that replacing Ser104 and Tyr107 by alanines within the conserved sequence motif SG*x*Y in loop 6 severely reduces both the inhibitory activity and the binding strength of PliI-Ah for Vp-iLys (Leysen *et al.*, 2011). The crystal structure of the Ml-iLys–PliI-Ah complex readily reveals the exact roles of these residues in the inhibitory mechanism: Ser104 forms a hydrogen bond to the catalytic Glu18 of Ml-iLys, while both Ser104 and Tyr107 make hydrogen bonds to Asn94 of the lysozyme (Fig. 1*c* and Table 2). The latter residue is part of substrate-binding site D.

As mentioned above, PliI-Ah loop 2 and loop 4 also take part in blocking the substrate-binding site. A multiple sequence alignment (Fig. 2) shows that Ser46 in loop 2 and Asp76 in loop 4 are highly conserved across the PliI family. In parallel with this, these residues are

found in the PliI-Ah–Ml-iLys interface: Ser46 makes a hydrogen bond to residue Tyr72 in the lysozyme, while Asp76 makes a salt bridge with the lysozyme residue Lys102 (Fig. 1*d*). We have further investigated the functional importance of Ser46 and Asp76 by creating corresponding alanine mutants of PliI-Ah and performing a cell-lysis assay in which their influence on the activity of Vp-iLys was compared with that of wild-type PliI-Ah. The single amino-acid replacements S46A and D76A retained 49 ± 6% and 41 ± 6% of the specific inhibitory activity of the wild type, respectively. Moreover, when these amino-acid substitutions were introduced, either individually or together, on top of the S104A/Y107A double mutation, the inhibitory activity was no longer detectable. This may be compared with the earlier observations that each of the single S104A and Y107A mutations does not influence the activity of PliI-Ah significantly, while the S104A/Y107A double mutant retains only 15 ± 3% of the wild-type activity (Leysen *et al.*, 2011). These results indicate that the conserved residues Ser46, Asp76, Ser104 and Tyr107 located in the protruding PliI loops all contribute to formation of the inhibitory complex. At the same time, a stable complex can still be formed even if one of these interactions is missing.

3.4. Comparative mechanism of action of i-type, c-type and g-type inhibitors on their target lysozymes

Here, we describe the molecular detail of i-type lysozyme inhibition by the PliI family. Previously, the interactions of both the MliC/PliC inhibitor family with their target c-type lysozymes and of the PliG family with the g-type lysozymes have been shown to involve a 'double key–lock' interface (Leysen *et al.*, 2013; Um *et al.*, 2013; Yum *et al.*, 2009). The first key–lock pair corresponds to a loop/strand insertion (MliC/PliC; Fig. 3*a*) or loop/helix insertion (PliG; Fig. 3*b*) of the inhibitor into the active groove of the lysozyme. The second key–lock pair in either case is formed by a loop of the lysozyme inserting into a pocket on the surface of the inhibitor. In contrast, the interaction of the Ivy inhibitor with the c-type lysozyme involves a simpler, single key–lock mechanism, with a single loop of Ivy inserting into the active site of the lysozyme (Fig. 3*c*; Abergel *et al.*, 2007). Our new results indicate that the PliI inhibition also involves a single key–lock pair, but the 'key' inserting into the substrate groove of the lysozyme is formed by three different PliI loops (Fig. 3*d*). The largest of these loops (loop 6) contains the conserved SG*x*Y motif. Together, the three loops form a 'ridge' which complements the extended shape of the substrate groove. Finally, our mutagenesis studies reveal that the PliI–iLys interaction is sufficiently strong to tolerate mutations in single key residues, but mutations of several residues typically result in both diminished strength of the interaction and loss of inhibitory efficiency. Parallel observations have previously been made for the PliG–gLys pair (Leysen *et al.*, 2012).

3.5. Suppressing lysozyme inhibitors as a novel antibacterial strategy

The important contribution of specific inhibitors of host lysozymes to bacterial proliferation has been supported by a number of findings, as recently reviewed in Callewaert *et al.* (2012). In particular, the contribution of lysozyme inhibitors to the virulence of avian pathogenic *E. coli* (APEC) was investigated in an *in vivo* study. It was shown that expression of MliC is required for the full virulence of APEC when injected into one-day-old chickens (Vanderkelen *et al.*, 2012). Correspondingly, lysozyme inhibitors may serve as targets for the development of novel antibacterial agents. The accumulated crystal structures of lysozyme–inhibitor complexes of several types (Fig. 3) provide a starting point for the rational design of such suppressor molecules. In particular, the 'lock' elements on the surface of the MliC/PliC and PliG inhibitors correspond to 'druggable' pockets. The first 'proof-of-concept' study in this direction was presented by Voet *et al.* (2011). Based on the crystal structure of *P. aeruginosa* MliC (MliC-Pa) in complex with hen egg-white lysozyme (HEWL), these authors identified small molecules capable of disrupting the interaction between HEWL and PliC from *Salmonella enterica* serovar Typhi. For PliI and Ivy inhibitors, however, designing small suppressor compounds would be problematic owing to the lack of the second key–lock interface and thus of a suitable pocket at the inhibitor side. Here, suppression of the inhibitory action might be achieved *via* the development of antibodies or nanobodies targeting appropriate locations on PliI or Ivy.

Access to the PROXIMA1 beamline at Synchrotron SOLEIL (France), supported by the BiostructX project 6131, and especially the help of Dr Andrew Thompson is gratefully acknowledged. We also thank Dr Stephen Weeks for feedback on the manuscript. SL received a doctoral fellowship from KU Leuven. JMVH held a doctoral fellowship of the Research Foundation-Flanders (FWO). This work was further supported by grants G.0363.08 from the FWO and METH/07/03 from KU Leuven.

References

Abergel, C., Monchois, V., Byrne, D., Chenivesse, S., Lembo, F., Lazzaroni, J. C. & Claverie, J.-1M. (2007). *Proc. Natl Acad. Sci. USA*, **104**, 6394–6399.
Adams, P. D. *et al.* (2010). *Acta Cryst.* D**66**, 213–221.
Callewaert, L., Aertsen, A., Deckers, D., Vanoirbeek, K. G., Vanderkelen, L., Van Herreweghe, J. M., Masschalck, B., Nakimbugwe, D., Robben, J., Michiels, C. W. & Ausubel, F. M. (2008). *PLoS Pathog.* **4**, e1000019.
Callewaert, L. & Michiels, C. W. (2010). *J. Biosci.* **35**, 127–160.
Callewaert, L., Van Herreweghe, J. M., Vanderkelen, L., Leysen, S., Voet, A. & Michiels, C. W. (2012). *Trends Microbiol.* **20**, 501–510.
Chen, V. B., Arendall, W. B., Headd, J. J., Keedy, D. A., Immormino, R. M., Kapral, G. J., Murray, L. W., Richardson, J. S. & Richardson, D. C. (2010). *Acta Cryst.* D**66**, 12–21.
Davis, K. M. & Weiser, J. N. (2011). *Infect. Immun.* **79**, 562–570.
Emsley, P. & Cowtan, K. (2004). *Acta Cryst.* D**60**, 2126–2132.
Engh, R. A. & Huber, R. (1991). *Acta Cryst.* A**47**, 392–400.
Evans, P. (2006). *Acta Cryst.* D**62**, 72–82.
Gille, C. & Frömmel, C. (2001). *Bioinformatics*, **17**, 377–378.
Kabsch, W. (2010). *Acta Cryst.* D**66**, 125–132.
Karplus, P. A. & Diederichs, K. (2012). *Science*, **336**, 1030–1033.
Krissinel, E. & Henrick, K. (2007). *J. Mol. Biol.* **372**, 774–797.
Kuwano, Y., Yoneda, K., Kawaguchi, Y. & Araki, T. (2013). *Acta Cryst.* F**69**, 1202–1206.

Kuwano, Y., Yoneda, K., Kawaguchi, Y., Araki, N. & Araki, T. (2013). *Biosci. Biotechnol. Biochem.* **77**, 2269–2277.
Leysen, S., Vanderkelen, L., Van Asten, K., Vanheuverzwijn, S., Theuwis, V., Michiels, C. W. & Strelkov, S. V. (2012). *J. Struct. Biol.* **180**, 235–242.
Leysen, S., Vanderkelen, L., Weeks, S. D., Michiels, C. W. & Strelkov, S. V. (2013). *Cell. Mol. Life Sci.* **70**, 1113–1122.
Leysen, S., Van Herreweghe, J. M., Callewaert, L., Heirbaut, M., Buntinx, P., Michiels, C. W. & Strelkov, S. V. (2011). *J. Mol. Biol.* **405**, 1233–1245.
McCoy, A. J., Grosse-Kunstleve, R. W., Adams, P. D., Winn, M. D., Storoni, L. C. & Read, R. J. (2007). *J. Appl. Cryst.* **40**, 658–674.
Monchois, V., Abergel, C., Sturgis, J., Jeudy, S. & Claverie, J.-M. (2001). *J. Biol. Chem.* **276**, 18437–18441.
Novotny, M., Seibert, M. & Kleywegt, G. J. (2007). *Acta Cryst.* D**63**, 270–274.
Pettersen, E. F., Goddard, T. D., Huang, C. C., Couch, G. S., Greenblatt, D. M., Meng, E. C. & Ferrin, T. E. (2004). *J. Comput. Chem.* **25**, 1605–1612.
Studier, F. W. (2005). *Protein Expr. Purif.* **41**, 207–234.
Um, S.-H., Kim, J.-S., Kim, K., Kim, N., Cho, H.-S. & Ha, N.-C. (2013). *Biochemistry*, **52**, 9385–9393.
Vanderkelen, L., Ons, E., Van Herreweghe, J. M., Callewaert, L., Goddeeris, B. M. & Michiels, C. W. (2012). *PLoS One*, **7**, e45954.
Vanderkelen, L., Van Herreweghe, J. M., Vanoirbeek, K. G., Baggerman, G., Myrnes, B., Declerck, P. J., Nilsen, I. W., Michiels, C. W. & Callewaert, L. (2011). *Cell. Mol. Life Sci.* **68**, 1053–1064.
Van Herreweghe, J. M. & Michiels, C. W. (2012). *J. Biosci.* **37**, 327–348.
Van Herreweghe, J. M., Vanderkelen, L., Callewaert, L., Aertsen, A., Compernolle, G., Declerck, P. J. & Michiels, C. W. (2010). *Cell. Mol. Life Sci.* **67**, 1177–1188.
Voet, A., Callewaert, L., Ulens, T., Vanderkelen, L., Vanherreweghe, J. M., Michiels, C. W. & De Maeyer, M. (2011). *Biochem. Biophys. Res. Commun.* **405**, 527–532.
Yum, S., Kim, M. J., Xu, Y., Jin, X. L., Yoo, H. Y., Park, J.-W., Gong, J. H., Choe, K.-M., Lee, B. L. & Ha, N.-C. (2009). *Biochem. Biophys. Res. Commun.* **378**, 244–248.